

Domain Agnostic Internal Distributions for Unsupervised Model Adaptation

Mohammad Rostami and Aram Galstyan

USC Information Science Institute, Los Angeles CA, USA rostamim@usc.edu

Abstract. We develop an algorithm for sequential adaptation of a classifier that is trained for a source domain to generalize in a unannotated target domain. We consider that the model has been trained on the source domain annotated data and then it needs to be adapted using the target domain unannotated data when the source domain data is not accessible. We align the distributions of the source and the target domains in a discriminative embedding space via an intermediate internal distribution. This distribution is estimated using the source data representations in the embedding space. We provide theoretical analysis and conduct extensive experiments on several benchmarks to demonstrate the proposed method is effective.

Keywords: Model Adaptation · Gaussian Mixture Model · Embedding.

1 Introduction

Advances in deep learning have led to significant performance improvement in a wide range of supervised learning tasks. Similar to other machine learning techniques, deep learning is vulnerable with respect to distributional shifts during the model execution time when the model is tested. Distributional shifts would lead to model performance degradation which makes model retraining, *i.e.*, *model adaptation*, inevitable to make the model generalizable again in new domains. Unfortunately, adapting deep neural networks is conditioned on availability of massive labeled datasets. This may not, however, be always feasible due to prohibitive costs of manual data annotation. A naive solution to improve model generalization is to finetune the previously trained neural network in the target domain. Despite requiring less annotated data and being effective in reducing the effect of domain shift, finetuning still requires target domain annotated data.

Domain adaptation is a similar problem in which only *unlabeled data* is accessible in the target domain [1], while the source domain labeled data is accessible at the same time. The goal in UDA is to leverage from the source domain data to acclimate the deep neural network to generalize well in the target domain. An effective approach for domain adaptation is to align distributions of both domains by mapping data into a latent domain-invariant space [2]. As a result, a classifier that is trained using the source labeled data features in this space will generalize well in the target domain. Recent domain adaptation methods model this latent space as the output of a shared deep encoder. The encoder

network is trained such that the source and the target domains share a similar distribution in its output. This training procedure has been implemented using either adversarial learning [3,4,5,6,7] or by directly minimizing the distance between the two distributions in the embedding [8,9,10,11,11,12,13]. Adversarial learning [14] has been used to extract features that are maximally discriminative in the source domain and at the same as indistinguishable as possible in the target domain. As a result, the distributions are aligned indirectly. Despite being effective, adversarial learning often requires delicate optimization initialization, architecture engineering, and careful selection of hyper-parameters to be stable [15]. Adversarial learning can also suffer from mode collapse [16]. In contrast, choosing the probability metric is the challenge for direct matching.

Most existing unsupervised domain adaptation (UDA) algorithms consider a joint learning setting, where the model is trained jointly on both the target domain unlabeled data and the source domain labeled data. As a result, these algorithms cannot be used for sequential model adaptation. Note that although a few source-free domain adaptation algorithms have been developed recently [17,18], these methods use adversarial learning to memorize the source domain to generate source domain pseudo-data points for model retraining which necessitates using additional networks, rather directly adapting the base classifier network. Our goal is to adapt the classifier model to generalize well in the target domain using solely the target domain unlabeled data. This setting can be considered as an improvement over using an off-the-shelf pre-trained model when unlabeled data in a source domain is available. Our approach also relaxes the necessity of sharing training data between the two domains for classic UDA.

Contributions: our main contribution is to develop a sequential model adaptation algorithm which is based on learning a parametric internal distribution for the source domain data distribution in a shared embedding space. This internally learned distribution is used to align the source and the target distributions. We approximate this multimodal distribution using a Gaussian mixture model (GMM). In order to adapt the model to work well in the target domain, we draw samples from this internal distribution and enforce the target domain to share the same distribution in the embedding space by minimizing the distance between the two distributions. We provide a theoretical justification for the proposed algorithm, by establishing an upperbound for the expected risk in the target domain, and demonstrating that our algorithm minimizes this upperbound. We conduct experiments on five standard benchmarks and observe that our algorithm compares favorably even with state-of-the-art UDA methods.

2 Background and Related Work

UDA is closely related to our learning setting. Several discrepancy measures have been used in the literature to align two distributions to address UDA. A group of methods match the first-order and the second order statistics of the source and the target domains. This includes methods that use the Maximum Mean Discrepancy (MMD) [8,10] and correlation alignment [19]. A more effec-

tive approach is to use a probability distance metric that captures distributional differences in higher order statistics. The Wasserstein distance (WD) [20,21] is such an example that is also a suitable metric for deep learning due to having non-vanishing gradients. This property is helpful because deep learning optimization problems are usually solved using the first-order optimization methods that rely on the objective function gradient. Damodaran et al. [21] used the WD for domain alignment in a UDA setting which led to considerable performance improvement compared to the methods that rely on matching only lower-order statistics [8,19]. In this work, we rely on the sliced Wasserstein distance (SWD) variant of WD [22] for domain alignment which possess similar properties but can be computed more efficiently due to its closed-form formulation.

Most existing UDA methods use a strong assumption. It is assumed that the source and the target domain data are accessible simultaneously and the model is trained jointly on two datasets. Sequential model adaptation can be considered as a more challenging setting when the source domain data is unavailable. By addressing this learning setting, we can also address UDA when the source domain data cannot be shared due to privacy or security concerns. This learning setting for domain adaptation has been explored for non-deep models [23,24,25]. However, these works address sequential model adaptation when the input distribution can be estimated with a parametric distribution and the base models have a small number of parameters. As a result, it is not trivial to extend the above works for the end-to-end training procedure of deep neural networks when deep learning is necessary for decent performance. Recently, adversarial learning has been used to address source-free DA [17,18], but these methods memorize the source domain using additional networks to generate a source pseudo-dataset that can be used as a surrogate for the real source dataset. Quite differently, we rely on an internally learned distribution by a base model for the source domain to align the two source and target domain distributions indirectly in an embedding space to adapt the base classifier sequentially. This approach eliminates the need for any additional network and processing the source data.

When a deep network is trained for solving a classification problem, the model would have decent performance only if the data points that belong to each class form a single cluster in an embedding space which is modeled by the network responses at higher layers. In other words, the source domain input distribution is transformed into a multimodal internal distribution, where each mode of the distribution encodes one of the classes. The internal distribution encodes the knowledge gained from supervised learning in the source domain. Domain shift occurs when changes in the input distribution lead to discrepancies between the transformed input distribution and the internally learned distribution. UDA can be addressed by aligning the target domain distribution internally with the source domain internal distribution. We estimate the internal distribution in the embedding space via a parametric Gaussian mixture model. We develop an algorithm for sequential model adaptation by enforcing the target domain to share the same internal distribution in the embedding space.

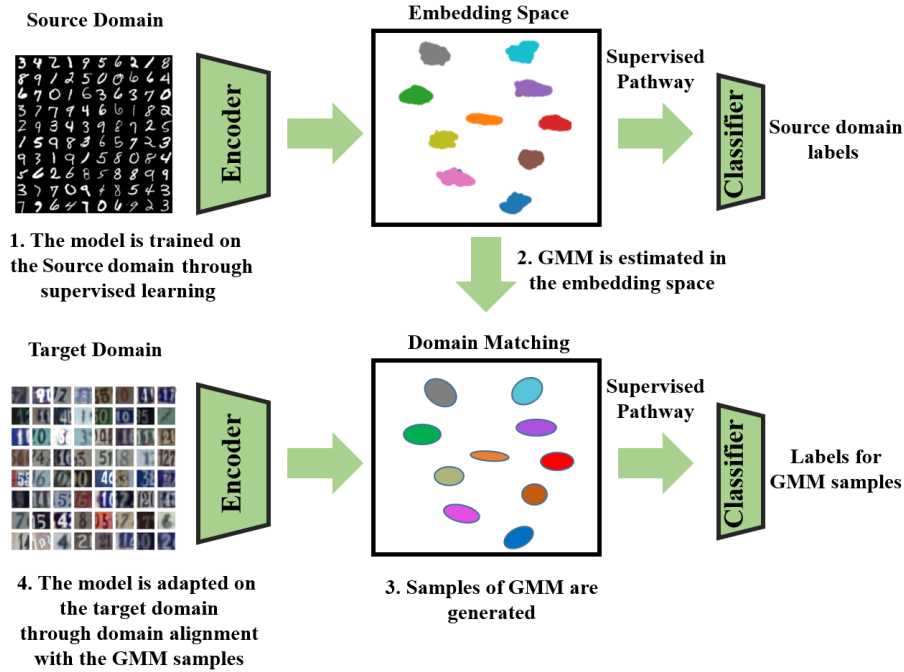


Fig. 1: Architecture of the proposed model adaptation framework.

3 Problem Statement

Consider a source domain \mathcal{S} which consists of the distribution $p_S(\mathbf{x})$ and the labeling function $f(\cdot) : \mathbb{R}^d \rightarrow \mathcal{Y} \subset \mathbb{R}^k$. Given a family of parametric functions $f_\theta : \mathbb{R}^d \rightarrow \mathcal{Y}$, e.g., a deep neural network with learnable parameter θ , our goal is to solve for an optimal model with minimum expected risk, i.e., $\mathbb{E}_{\mathbf{x}^s \sim p_S(\mathbf{x})}(\mathcal{L}(f_\theta(\mathbf{x}^s), f(\mathbf{x}^s)))$, where $\mathcal{L}(\cdot)$ is a proper loss function. To this end, we are given a labeled dataset $\mathcal{D}_S = (\mathbf{X}_S, \mathbf{Y}_S)$ in the source domain, with $\mathbf{X}_S = [\mathbf{x}_1^s, \dots, \mathbf{x}_N^s] \in \mathcal{X} \subset \mathbb{R}^{d \times N}$ and $\mathbf{Y}_S = [\mathbf{y}_1^s, \dots, \mathbf{y}_N^s] \in \mathcal{Y} \subset \mathbb{R}^{k \times N}$, where the data points are drawn i.i.d. $\mathbf{x}_i^s \sim p_S(\mathbf{x})$. Given a sufficiently large enough number of labeled data points, we can solve for the optimal parameters using the standard empirical risk minimization (ERM): $\hat{\theta} = \arg \min_{\theta} \hat{e}_\theta(\mathbf{X}_S, \mathbf{Y}_S, \mathcal{L}) = \arg \min_{\theta} \sum_i \mathcal{L}(f_\theta(\mathbf{x}_i^s), \mathbf{y}_i^s)$, as a surrogate for the true risk. Consider that after training on the source domain, we also encounter a target domain sequentially with an unlabeled dataset $\mathcal{D}_T = (\mathbf{X}_T)$, where $\mathbf{X}_T = [\mathbf{x}_1^t, \dots, \mathbf{x}_M^t] \in \mathbb{R}^{d \times M}$ and $\mathbf{x}_i^t \sim p_T(\mathbf{x})$. As a result, using ERM is not feasible in the target domain. We know a priori that the two domains share the same classes but despite this relation, distributional discrepancy exists between the domains, i.e., $p_S \neq p_T$. This leads to poor generalization of $f_{\hat{\theta}}$ in the target domain due to domain shift. Our goal is

to adapt the classifier $f_{\hat{\theta}}$ using solely the dataset $\mathcal{D}_{\mathcal{T}}$ such that it generalizes well in the target domain when the source dataset is not accessible (see Figure 1).

In order to circumvent the challenge of distributional gap between the two domains, we can decompose the mapping $f_{\theta}(\cdot)$ into a deep encoder $\phi_v(\cdot) : \mathcal{X} \rightarrow \mathcal{Z} \subset \mathbb{R}^p$ and a classifier subnetwork $h_w(\cdot) : \mathcal{Z} \rightarrow \mathcal{Y}$ such that $f_{\theta} = h_w \circ \phi_v$, where $\theta = (w, v)$. Here, \mathcal{Z} denotes an intermediate embedding space between the input space and the label space in which we assume that the classes have become geometrically separable. Given $\hat{\theta}$ and $\mathcal{D}_{\mathcal{T}}$, if we adapt ϕ_v such that the discrepancy between the source and target distributions, i.e., the distance between $\phi(p_S(x^s))$ and $\phi(p_{\mathcal{T}}(x^t))$, is minimized in the embedding space (making the embedding domain agnostic), then the classifier h_w will generalize well on the target domain, despite being trained using only the source labeled data points. Many prior classic UDA algorithms use this strategy but implement it by assuming that \mathcal{D}_S is always accessible. This makes computing the distance between the distributions $\phi(p_S(x^s))$ and $\phi(p_{\mathcal{T}}(x^t))$ feasible and hence UDA reduces to selecting a proper probability metric and then solving a typical deep learning minimization problem [8,10,21,20,21]. The major challenge in the sequential model adaptation setting is that as opposed to UDA, the term $\phi(p_S(x^s))$ cannot be computed and we need a new approach to estimate it.

4 Proposed Algorithmic Solution

We propose to solve the challenge of sequential model adaptation through aligning the source and the target distribution indirectly via an intermediate internally learned distribution in the embedding space. We set a softmax function at the output of the encoder just before passing data representations into the classifier subnetwork. As a result, the classifier can be assumed as a maximum *a posteriori* (MAP) estimator which assigns a membership probability distribution to any given data point. This means that when an optimal model is trained for the source domain, the encoder would transform the source distribution into a multi-modal distribution $p_J(z)$ with k components in the embedding space (see Figure 1, right). This occurs because the classes should become separable in the embedding space as the result of learning for a generalizable model. This internal distribution is a multimodal distribution in which each distribution mode would capture one of the classes. If we update the model such that the internal distribution remains stable in the target domain after model adaptation, i.e., the source and the target domain would share similar internal distributions in the embedding space, then the classifier subnetwork would generalize well in the target domain due to negligible domain gap in the embedding space.

The empirical version of the internal distribution is encoded by the source data samples $\{(\phi_v(x_i^s), y_i^s)\}_{i=1}^N$. We consider that $p_J(z)$ is a GMM as:

$$p_J(z) = \sum_{j=1}^k \alpha_j \mathcal{N}(z | \mu_j, \Sigma_j), \quad (1)$$

where α_j denote mixture weights, i.e., prior probability for each class, μ_j and Σ_j denote the mean and co-variance for each component. Since we have labeled data points, we can compute the GMM parameters using MAP estimates. Let \mathcal{S}_j denote the support set for class j in the training dataset, i.e., $\mathcal{S}_j = \{(\mathbf{x}_i^s, \mathbf{y}_i^s) \in \mathcal{D}_S \mid \arg \max \mathbf{y}_i^s = j\}$. Then, the MAP estimate for the parameters would be:

$$\begin{aligned} \hat{\alpha}_j &= \frac{|\mathcal{S}_j|}{N}, \quad \hat{\mu}_j = \sum_{(\mathbf{x}_i^s, \mathbf{y}_i^s) \in \mathcal{S}_j} \frac{1}{|\mathcal{S}_j|} \phi_v(\mathbf{x}_i^s), \\ \hat{\Sigma}_j &= \sum_{(\mathbf{x}_i^s, \mathbf{y}_i^s) \in \mathcal{S}_j} \frac{1}{|\mathcal{S}_j|} (\phi_v(\mathbf{x}_i^s) - \hat{\mu}_j)^\top (\phi_v(\mathbf{x}_i^s) - \hat{\mu}_j). \end{aligned} \quad (2)$$

Our major idea is to use this internal distributional estimate to circumvent the major challenge of sequential UDA. In order to adapt the model to work well for the target domain, we update the model such that the encoder matches the target distribution into the internal distribution in the embedding space. To this end, we can draw random samples from the internal distributional estimate and generate a labeled pseudo-dataset: $\hat{\mathcal{D}} = (\mathbf{Z}_{\mathcal{P}}, \mathbf{Y}_{\mathcal{P}})$, where $\mathbf{Z}_{\mathcal{P}} = [z_1^p, \dots, z_{N_p}^p] \in \mathbb{R}^{p \times N_p}$, $\mathbf{Y}_{\mathcal{P}} = [\mathbf{y}_1^p, \dots, \mathbf{y}_{N_p}^p] \in \mathbb{R}^{k \times N_p}$, $z_i^p \sim \hat{p}_j(z)$, and the labels are ascribed according to the classifier subnetwork prediction. To generate a clean pseudo-dataset, we also set a threshold τ and include only those generated samples for which the classifier prediction confidence is greater than τ . The sequential UDA problem then reduces to solving the alignment problem as the following:

$$\min_{v, w} \sum_{i=1}^N \mathcal{L}(h_w(z_i^p), \mathbf{y}_i^p) + \lambda D(\phi_v(p_{\mathcal{T}}(\mathbf{X}_{\mathcal{T}})), \hat{p}_j(\mathbf{Z}_{\mathcal{P}})), \quad (3)$$

where $D(\cdot, \cdot)$ denotes a probability metric to measure the distributional discrepancy, and λ is a trade-off parameter between the terms (see Figure 1, left).

The first term in Eq. (3) is to ensure that the classifier continues to perform well on the internal distribution (note that the pseudo-dataset approximates this distribution). The second term is the domain alignment matching loss which enforces the target domain to share the internal distribution in the embedding space. The major remaining question is selection of the distribution metric. We choose SWD metric [20] to compute $D(\cdot, \cdot)$ due to its suitability for deep learning due to possessing non-vanishing gradients when two distributions have non-overlapping supports [26,22]. SWD inherits this property from WD, yet the advantage of using SWD over WD is that SWD can be computed efficiently using a closed form solution. Additionally, empirical version of SWD can be computed using the samples that are drawn from the corresponding two distributions, as it is the case in Eq. (3). Hence, Eq. (3) can be solved using first-order optimization techniques (see Appendices for more details on properties of SWD). Our proposed solution, named Sequential Model Adaptation Using Internal distribution (SMAUI), is presented and visualized in Algorithm 1. Figure 1 also presents the high-level implementation of our algorithm.

5 Theoretical Analysis

Algorithm 1 SDAUP (λ, ITR)

- 1: **Initial Training:**
 - 2: **Input:** source dataset $\mathcal{D}_S = (\mathbf{X}_S, \mathbf{Y}_S)$,
 - 3: **Training on Source Domain:**
 - 4: $\hat{\theta}_0 = (\hat{w}_0, \hat{v}_0) = \arg \min_{\theta} \sum_i \mathcal{L}(f_{\theta}(\mathbf{x}_i^s), \mathbf{y}_i^s)$
 - 5: **Internal Distribution Estimation:**
 - 6: Use Eq. (2) and estimate α_j, μ_j , and Σ_j
 - 7: **Model Adaptation:**
 - 8: **Input:** target dataset $\mathcal{D}_T = (\mathbf{X}_T)$
 - 9: **Pseudo-Dataset Generation:**
 - 10: $\hat{\mathcal{D}}_P = (\mathbf{Z}_P, \mathbf{Y}_P) = ([z_1^p, \dots, z_N^p], [y_1^p, \dots, y_N^p])$,
 - 11: where:
 - 12: $z_i^p \sim \hat{p}_j(z), 1 \leq i \leq N_p$
 - 13: $y_i^p = \arg \max_j \{h_{\hat{w}_0}(z_i^p)\}$
 - 14: **for** $itr = 1, \dots, ITR$ **do**
 - 15: draw data batches from $\hat{\mathcal{D}}_T$ and $\hat{\mathcal{D}}_P$
 - 16: Update the model by solving Eq. (3)
 - 17: **end for**
-

We demonstrate that our algorithm optimizes an upperbound for the target domain expected risk. We treat the embedding space as the hypothesis space within the standard PAC-learning in our analysis. We consider the hypothesis class for PAC-learning to be the set of classifier subnetworks parameterized by w , $\mathcal{H} = \{h_w(\cdot) | h_w(\cdot) : \mathcal{Z} \rightarrow \mathbb{R}^k, v \in \mathbb{R}^V\}$. We denote the observed risk on the source and the target domains by e_S and e_T , respectively. Also, let $\hat{\mu}_S = \frac{1}{N} \sum_{n=1}^N \delta(\phi_v(\mathbf{x}_n^s))$ and $\hat{\mu}_T = \frac{1}{M} \sum_{m=1}^M \delta(\phi_v(\mathbf{x}_m^t))$ denote the empirical source and the empirical target distributions in the embedding space. These distributions are computed using the representations of the training data in the embedding space. Similarly, let $\hat{\mu}_P = \frac{1}{N_p} \sum_{q=1}^{N_p} \delta(z_q^p)$ denote the empirical internal distribution built using the pseudo-dataset. Moreover, let h_{w^*} denote the optimal model that minimizes the combined source and target risks $e_C(w^*)$, i.e.

$w^* = \arg \min_w e_C(w) = \arg \min_w \{e_S + e_T\}$. In the presence of enough labeled target domain data, this is the best model that can be learned jointly on both domains. Finally, since we generate a clean pseudo-dataset, we can let $\tau = \mathbb{E}_{z \sim p_j(\hat{z})} (\mathcal{L}(h(z), h_{\hat{w}_0}(z)))$ as the expected risk of the optimal model that is trained using the source domain data on the generated pseudo-dataset using the GMM. We provide the following theorem to justify our algorithm.

Theorem 1: Consider that we generate a pseudo-dataset using the estimate for the internally learned distribution and update the model sequentially using the algorithm 1. Then, the following upperbound for the target domain holds:

$$\begin{aligned}
 e_T \leq & e_S + W(\hat{\mu}_S, \hat{\mu}_P) + W(\hat{\mu}_T, \hat{\mu}_P) + (1 - \tau) + e_C(w^*) \\
 & + \sqrt{(2 \log(\frac{1}{\zeta}) / \zeta)} (\sqrt{\frac{1}{N}} + \sqrt{\frac{1}{M}} + 2\sqrt{\frac{1}{N_p}}),
 \end{aligned} \tag{4}$$

where $W(\cdot, \cdot)$ denotes the WD distance and ζ is a constant number which depends on the properties loss function $\mathcal{L}(\cdot)$.

Proof: The complete proof is included in the Appendix.

We can use Theorem 1 to explain why our algorithm can adapt the model that is trained using the source domain to generalize well on the target domain. We can see that SMAUI algorithm minimizes the upperbound of the target domain risk as given in Eq. (4). The first three terms are minimized directly. The source risk e_S is minimized through the initial training on the source domain prior to the model adaptation step. We minimize the second term in the upperbound of Eq. (4) by intentionally fitting a GMM distribution on the source domain distribution in the embedding. We note that this term is small if the source domain distribution can be fit well with a GMM distribution in reality. Hence, this is a constraint for applicability of our method. Note, however, all the parametric learning methods face a similar limitation and this is not particular to our algorithm. The third term is minimized directly because it is the second term in the objective function of Eq. (3). The fourth and fifth terms are not minimized by our algorithm, rather state conditions under which the algorithm would work. The term $(1 - \tau)$ is small if we set $\tau \approx 1$ to generate a clean pseudo-dataset and cancel out the outliers. We note that if τ is chosen very close to 1, then the pseudo-dataset samples would all be close to the mean and hence pseudo-dataset will not capture the higher-order moments of the internal distribution. The term $e_C(w^*)$ is a constant term. This term will be small if the domains are related, i.e., share the same classes, and in presence of the target labeled data, the base model can be trained to work well on both domains. This means that aligning the distributions in the embedding must be a possibility for our algorithm to work. Finally, the last term in Eq. (4) is a constant term that merely states that in order to train a good model, we need sufficiently large source and target datasets and also generate a large pseudo-dataset. From the above discussion, we conclude assuming that the domains are related and applicability of the GMM estimate, SMAUI minimizes all the remaining terms in the upperbound of Eq. (4), which would in term lead to a smaller true risk on the target domain after the model adaptation process.

6 Experimental Validation

To the best of our knowledge, sequential model adaptation is quite an unexplored learning setting. For this reason, we compare our algorithm against several recently developed UDA algorithms using benchmark UDA tasks due to closeness of the UDA learning setting to the sequential model adaptation setting. In order to demonstrate effectiveness of our algorithm, we consider different UDA tasks in terms of difficulty and the base network structure. Our implemented code is available at: <https://github.com/mrostami1366/SequentialUDA>.

6.1 Datasets

We validate our method on five standard benchmark set of UDA tasks.

Digit recognition tasks: MNIST (\mathcal{M}), USPS (\mathcal{U}), and Street View House Numbers, i.e., SVHN (\mathcal{S}), datasets are used as the three digit recognition do-

mains. Following the the UDA literature, we report performance on the three UDA tasks: $\mathcal{M} \rightarrow \mathcal{U}$, $\mathcal{U} \rightarrow \mathcal{M}$, and $\mathcal{S} \rightarrow \mathcal{M}$ tasks.

Office-31 Detest: this dataset is a visual recognition dataset with a total of 4,652 images which are categorized into ten classes in three distinct domains: Amazon (\mathcal{A}), Webcam (\mathcal{W}) and DSLR (\mathcal{D}). We report performance on the six pair-wise definable UDA tasks among these domains.

ImageCLEF-DA Dataset: this image classification dataset is a generated using the 12 shared classes between the Caltech-256 (\mathcal{C}), the ILSVRC 2012 (\mathcal{I}), and the Pascal VOC 2012 (\mathcal{P}) visual recognition datasets. Each class has 50 images which results in 600 images for each domain. We perform experiments on the six possible UDA tasks.

Office-Caltech Dataset: this dataset is generated using the 10 shared classes between the Office-31 and Caltech-256 datasets. There are four domains \mathcal{A} , \mathcal{C} , \mathcal{D} , \mathcal{W} with 12 definable tasks and 2533 images in total. These tasks help to measure the cross-dataset adaptation performance.

VisDA-2017: the goal for this dataset is to train a model on a synthetic domain and adapt it to work well on real natural images. The synthetic images are generated by renderings of 3D models from different angles and with different lightning conditions across 12 classes with over 280K images.

6.2 Empirical Evaluation:

Since sequential model adaptation is not a well-explored problem, we follow the UDA literature for evaluation due to the topic proximity. For this reason, we use the metrics and the features used in the UDA literature for fair comparison. We use the VGG16 network as the base model for the digit recognition tasks. The network is initialized with random weights. We use the Decaf6 features for the Office-Caltech tasks. For the rest of tasks, we use the ResNet-50 network which is pre-trained on the ImageNet dataset as the backbone of the network. We set $\tau = 0.99$ and $\lambda = 10^{-3}$. Our ablative study explain the reason for these choices.

We report the average classification rate on the target domain and the standard deviation based on ten runs for each UDA task. We train the base model using the source labeled data. We report the performance of the model before adaptation as a baseline which also demonstrates the effect of domain shift. Then we adapt the model using the target unlabeled data using SMAUI algorithm and report the target domain performance. In our Tables, bold font denotes the best performance. The baseline performance before model adaptation is reported in the first row, then the UDA methods based on adversarial learning, then the UDA methods based on direct matching which are separated by a line in the middle, followed by our result in the last row of the tables.

In our comparison, we include both pioneer and recent works to be representative of the UDA literature. We include methods that are based on adversarial learning: GtA [4], DANN [27], ADDA [28], MADA [5], SymNets [6], CDAN [7], and MMAN [29]. We have also included methods based on direct distribution matching: DAN [8], DRCN [30], CORAL [31], RevGrad [9], CAN [11], JAN [10], WDGRL [32], JDDA [33], and ETD [34]. We also compare against UDAwSD [18]

and SHOT [35] which are source-free UDA methods. For each dataset, we include results of the works for which the original paper has used that dataset.

For more details on the experimental setup, please refer to the Appendix.

6.3 Results

Results for the digit recognition tasks are reported in Table 1. Despite the sequential training regime, we observe SMAUI outperforms the other methods in one of these tasks and its performance is quite competitive in the other two tasks. SMAUI leads to strong results compared to the joint UDA methods because stabilizing the internal distribution for both domain would mitigate domain shift. We also observe that performance of the methods based on direct probability match has improved recently which might be because of using secondary mechanisms to improve generalization in addition to distribution matching.

Table 2 summarizes the results for Office-31 dataset. We see in two of the tasks SMAUI leads to the best results and for the rest of the tasks is still competitive. Note, however, it seems there is no clear winner algorithm across the tasks of this dataset. This may be because some labels in this dataset are noisy and some images contain objects that belong to other classes [36]. The approach we use to align the two distributions is vulnerable with respect to this label pollution which makes aligning the distributions class-conditionally more challenging. We conclude that label pollution can degrade the performance of SMAUI.

Results for UDA tasks of the ImageCLEF-DA dataset are reported in Table 3. We see that although SMAUI does not use the source samples during model adaptation, it leads to a significant performance boost over the prior methods for this dataset. This may be because the Caltech-256, the ILSVRC 2012, and the Pascal VOC 2012 datasets have the equal size and the domains are balanced across the classes. As a result, matching the source and the target distributions to the same internal multi-modal distribution is more straightforward for the ImageCLEF-DA dataset. Note that we rely on empirical distributions for alignment and as a result balanced datasets represent true distributions better.

We have reported results for the Office-Caltech dataset in Table 4. We note that SMAUI leads to a relatively competitive performance on the tasks and in terms of average performance outperforms the listed UDA methods in this dataset. We conclude that addition of the Caltech-256 dataset might have helped mitigating the effect of label pollution which has improved our performance.

Results for VisDA task is presented in Table 5. We observe a significant boost in performance for VisDA task. From inspecting Tables 1–5, we conclude that there is no single method with the best performance on all the tasks. This is natural because these datasets are diverse in terms of difficulty, cross-domain gap, dataset size, label-pollution, etc, and any particular method may be more vulnerable in special cases. However, we note that although these UDA methods should serve an upperbound for SMAUI- as a sequential model adaptation method- SMAUI works reasonably well on all the domain adaptation tasks with state-of-the-art performance on many of the tasks. These results demonstrate that although our motivation was to address sequential model adaptation,

| Method | $\mathcal{M} \rightarrow \mathcal{U}$ | $\mathcal{U} \rightarrow \mathcal{M}$ | $\mathcal{S} \rightarrow \mathcal{M}$ | Method | $\mathcal{M} \rightarrow \mathcal{U}$ | $\mathcal{U} \rightarrow \mathcal{M}$ | $\mathcal{S} \rightarrow \mathcal{M}$ |
|-------------|---------------------------------------|---------------------------------------|---------------------------------------|-------------|---------------------------------------|---------------------------------------|---------------------------------------|
| GtA [4] | 92.8 ± 0.9 | 90.8 ± 1.3 | 92.4 ± 0.9 | CDAN [7] | 93.9 | 96.9 | 88.5 |
| ADDA [28] | 89.4 ± 0.2 | 90.1 ± 0.8 | 76.0 ± 1.8 | CyCADA [37] | 95.6 ± 0.2 | 96.5 ± 0.1 | 90.4 ± 0.4 |
| RevGrad [9] | 77.1 ± 1.8 | 73.0 ± 2.0 | 73.9 | JDDA [33] | - | 97.0 ± 0.2 | 93.1 ± 0.2 |
| DRCN [30] | 91.8 ± 0.1 | 73.7 ± 0.4 | 82.0 ± 0.2 | OPDA [20] | 70.0 | 60.2 | - |
| ETD [34] | 96.4 ± 0.3 | 96.3 ± 0.1 | 97.9 ± 0.4 | MML [38] | 77.9 | 60.5 | 62.9 |
| Source Only | 90.1 ± 2.6 | 80.2 ± 5.7 | 67.3 ± 2.6 | SMAUI | 92.2 ± 0.5 | 98.2 ± 0.2 | 92.6 ± 1.0 |

Table 1: Classification accuracy for UDA tasks between MINIST, USPS, and SVHN digit recognition datasets.

| Method | $\mathcal{A} \rightarrow \mathcal{W}$ | $\mathcal{D} \rightarrow \mathcal{W}$ | $\mathcal{W} \rightarrow \mathcal{D}$ | $\mathcal{A} \rightarrow \mathcal{D}$ | $\mathcal{D} \rightarrow \mathcal{A}$ | $\mathcal{W} \rightarrow \mathcal{A}$ | Average |
|-----------------|---------------------------------------|---------------------------------------|---------------------------------------|---------------------------------------|---------------------------------------|---------------------------------------|-------------|
| Source Only [3] | 68.4 ± 0.2 | 96.7 ± 0.1 | 99.3 ± 0.1 | 68.9 ± 0.2 | 62.5 ± 0.3 | 60.7 ± 0.3 | 75.6 |
| GtA [4] | 89.5 ± 0.5 | 97.9 ± 0.3 | 99.8 ± 0.4 | 87.7 ± 0.5 | 72.8 ± 0.3 | 71.4 ± 0.4 | 86.5 |
| DANN [27] | 82.0 ± 0.4 | 96.9 ± 0.2 | 99.1 ± 0.1 | 79.7 ± 0.4 | 68.2 ± 0.4 | 67.4 ± 0.5 | 82.2 |
| ADDA [28] | 86.2 ± 0.5 | 96.2 ± 0.3 | 98.4 ± 0.3 | 77.8 ± 0.3 | 69.5 ± 0.4 | 68.9 ± 0.5 | 82.8 |
| SymNets [6] | 90.8 ± 0.1 | 98.8 ± 0.3 | 100.0 ± .0 | 93.9 ± 0.5 | 74.6 ± 0.6 | 72.5 ± 0.5 | 88.4 |
| MADA [5] | 82.0 ± 0.4 | 96.9 ± 0.2 | 99.1 ± 0.1 | 79.7 ± 0.4 | 68.2 ± 0.4 | 67.4 ± 0.5 | 82.2 |
| CDAN [7] | 93.1 ± 0.2 | 98.2 ± 0.2 | 100.0 ± 0.0 | 89.8 ± 0.3 | 70.1 ± 0.4 | 68.0 ± 0.4 | 86.6 |
| UDAwSD [18] | 93.7 ± 0.2 | 98.5 ± 0.1 | 99.8 ± 0.2 | 92.7 ± 0.4 | 75.3 ± 0.5 | 77.8 ± 0.1 | 89.6 |
| DAN [8] | 80.5 ± 0.4 | 97.1 ± 0.2 | 99.6 ± 0.1 | 78.6 ± 0.2 | 63.6 ± 0.3 | 62.8 ± 0.2 | 80.4 |
| DRCN [30] | 72.6 ± 0.3 | 96.4 ± 0.1 | 99.2 ± 0.3 | 67.1 ± 0.3 | 56.0 ± 0.5 | 72.6 ± 0.3 | 77.7 |
| RevGrad [9] | 82.0 ± 0.4 | 96.9 ± 0.2 | 99.1 ± 0.1 | 79.7 ± 0.4 | 68.2 ± 0.4 | 67.4 ± 0.5 | 82.2 |
| CAN [11] | 94.5 ± 0.3 | 99.1 ± 0.2 | 99.8 ± 0.2 | 95.0 ± 0.3 | 78.0 ± 0.3 | 77.0 ± 0.3 | 90.6 |
| JAN [10] | 85.4 ± 0.3 | 97.4 ± 0.2 | 99.8 ± 0.2 | 84.7 ± 0.3 | 68.6 ± 0.3 | 70.0 ± 0.4 | 85.8 |
| JDDA [33] | 82.6 ± 0.4 | 95.2 ± 0.2 | 99.7 ± 0.0 | 79.8 ± 0.1 | 57.4 ± 0.0 | 66.7 ± 0.2 | 80.2 |
| ETD [34] | 92.1 | 100.0 | 100.0 | 88.0 | 71.0 | 67.8 | 86.2 |
| SHOT [35] | 91.2 | 98.3 | 99.9 | 90.6 | 72.5 | 71.4 | 87.3 |
| SMAUI | 97.8 ± 2.1 | 95.6 ± 0.5 | 99.1 ± 0.3 | 97.8 ± 1.7 | 68.2 ± 4.5 | 71.7 ± 3.6 | 88.4 |

Table 2: Classification accuracy for UDA tasks for Office-31 dataset.

SMAUI can also be used as a standard joint training UDA algorithm with competitive results. Moreover, it can also be used as a source-free domain adaptation algorithm for preserving privacy. Note that SMAUI mostly outperforms the recently developed source-free UDA methods. We hope that the emergence of other sequential model adaptation methods would allow comparing our results against methods which are more similar to our work in the future.

6.4 Analysis and Ablative Studies

To demonstrate that SMAUI algorithm implements what we anticipated and to provide a better intuition about its effectiveness, we have used the UMAP [41] visualization tool to reduce the dimension of the data representations in the embedding space to two for 2D visualization purpose. Figure 2 represents the testing data splits of the source and the target domains and samples of the internal distribution for the $\mathcal{S} \rightarrow \mathcal{M}$ digit recognition task. In this figure, each point represents one data point and each color represents one of the ten digit

| Method | $\mathcal{I} \rightarrow \mathcal{P}$ | $\mathcal{P} \rightarrow \mathcal{I}$ | $\mathcal{I} \rightarrow \mathcal{C}$ | $\mathcal{C} \rightarrow \mathcal{I}$ | $\mathcal{C} \rightarrow \mathcal{P}$ | $\mathcal{P} \rightarrow \mathcal{C}$ | Average |
|-----------------|---------------------------------------|---------------------------------------|---------------------------------------|---------------------------------------|---------------------------------------|---------------------------------------|-------------|
| Source Only [3] | 74.8 \pm 0.3 | 83.9 \pm 0.1 | 91.5 \pm 0.3 | 78.0 \pm 0.2 | 65.5 \pm 0.3 | 91.2 \pm 0.3 | 80.8 |
| DANN [27] | 82.0 \pm 0.4 | 96.9 \pm 0.2 | 99.1 \pm 0.1 | 79.7 \pm 0.4 | 68.2 \pm 0.4 | 67.4 \pm 0.5 | 82.2 |
| SymNets [6] | 80.2 \pm 0.3 | 93.6 \pm 0.2 | 97.0 \pm 0.3 | 93.4 \pm 0.3 | 78.7 \pm 0.3 | 96.4 \pm 0.1 | 89.9 |
| MADA [5] | 75.0 \pm 0.3 | 87.9 \pm 0.2 | 96.0 \pm 0.3 | 88.8 \pm 0.3 | 75.2 \pm 0.2 | 92.2 \pm 0.3 | 85.9 |
| CDAN [7] | 76.7 \pm 0.3 | 90.6 \pm 0.3 | 97.0 \pm 0.4 | 90.5 \pm 0.4 | 74.5 \pm 0.3 | 93.5 \pm 0.4 | 87.1 |
| DAN [8] | 74.5 \pm 0.4 | 82.2 \pm 0.2 | 92.8 \pm 0.2 | 86.3 \pm 0.4 | 69.2 \pm 0.4 | 89.8 \pm 0.4 | 82.4 |
| RevGrad [9] | 75.0 \pm 0.6 | 86.0 \pm 0.3 | 96.2 \pm 0.4 | 87.0 \pm 0.5 | 74.3 \pm 0.5 | 91.5 \pm 0.6 | 85.0 |
| JAN [10] | 76.8 \pm 0.4 | 88.0 \pm 0.2 | 94.7 \pm 0.2 | 89.5 \pm 0.3 | 74.2 \pm 0.3 | 91.7 \pm 0.3 | 85.7 |
| ETD [34] | 81.0 | 91.7 | 97.9 | 93.3 | 79.5 | 95.0 | 89.7 |
| SMAUI | 88.7 \pm 1.2 | 99.5 \pm 0.2 | 100 \pm 0.0 | 94.9 \pm 0.3 | 88.8 \pm 0.9 | 99.8 \pm 0.0 | 95.3 |

Table 3: Classification accuracy for UDA tasks for ImageCLEF-DA dataset.

| Method | A \rightarrow C | A \rightarrow D | A \rightarrow W | W \rightarrow A | W \rightarrow D | W \rightarrow C | D \rightarrow A | D \rightarrow W | D \rightarrow C | C \rightarrow A | C \rightarrow W | C \rightarrow D | Average |
|-------------|-------------------|-------------------|-------------------|-------------------|-------------------|-------------------|-------------------|-------------------|-------------------|-------------------|-------------------|-------------------|-------------|
| Source Only | 84.6 | 81.1 | 75.6 | 79.8 | 98.3 | 79.6 | 84.6 | 96.8 | 80.5 | 92.4 | 84.2 | 87.7 | 85.4 |
| DANN [27] | 87.8 | 82.5 | 77.8 | 83.0 | 100 | 81.3 | 84.7 | 99.0 | 82.1 | 93.3 | 89.5 | 91.2 | 87.7 |
| MMAN [29] | 88.7 | 97.5 | 96.6 | 94.2 | 100 | 89.4 | 94.3 | 99.3 | 87.9 | 93.7 | 98.3 | 98.1 | 94.6 |
| RevGrad [9] | 85.7 | 89.2 | 90.8 | 93.8 | 98.7 | 86.9 | 90.6 | 98.3 | 83.7 | 92.8 | 88.1 | 87.9 | 88.9 |
| DAN [8] | 84.1 | 91.7 | 91.8 | 92.1 | 100 | 81.2 | 90.0 | 98.5 | 80.3 | 92.0 | 90.6 | 89.3 | 90.1 |
| CORAL [31] | 86.2 | 91.2 | 90.5 | 88.4 | 100 | 88.6 | 85.8 | 97.9 | 85.4 | 93.0 | 92.6 | 89.5 | 90.8 |
| WDGRL [32] | 87.0 | 93.7 | 89.5 | 93.7 | 100 | 89.4 | 91.7 | 97.9 | 90.2 | 93.5 | 91.6 | 94.7 | 92.7 |
| SMAUI | 99.9 | 100.0 | 96.7 | 96.8 | 100 | 94.4 | 84.8 | 93.4 | 91.8 | 98.8 | 80.4 | 91.4 | 94.0 |

Table 4: Performance comparison for UDA tasks of Office-Caltech dataset.

| Task | JAN [10] | DJT [21] | GtA [4] | SimNet [39] | CDAN [7] | MCD [40] | SMAUI |
|--------------------------|----------|----------|---------|-------------|----------|----------|----------------------------------|
| Syn. \rightarrow Real. | 61.6 | 66.9 | 69.5 | 69.6 | 70.0 | 71.9 | 76.9 \pm 0.7 |

Table 5: Classification accuracy for the VisDA UDA task.

classes. Comparing Figures 2a and 2b, we can see that the high-confidence internal GMM distribution samples approximate the source domain distribution reasonably well. Figure 2c denotes that the target domain samples are separable prior to adaptation to some extent due to domain similarity, but we can observe more regions with overlapped classes, i.e., less separability, that lead to performance degradation. This is due to distributional gap between the two domains. Figure 2d denotes that SMAUI algorithm has aligned the source and the target distributions using the intermediate internal distribution. Figure 2 empirically confirms the results that we could deduce from Theorem 1 because upperbound minimization has led to improved generalization on the target domain.

For a class-level analysis of effect of model adaptation, Figures 3a–3d visualize the confusion matrices for the classifier with explanations in the caption. We can see in Figure 3b that domain shift causes confusion between digit classes that are in visually similar classes, e.g., digits “3” and “8” or digits “4”, “7”, and “9”. As seen in Figure 3c, the confusion is reduced for all classes using SMAUI algorithm. Comparing Figure 3c with Figures 3a and 3d, we see that the initial confusions between the classes in the source domain translate into the target domain, despite the fact that the target domain (\mathcal{M}) is an easier problem

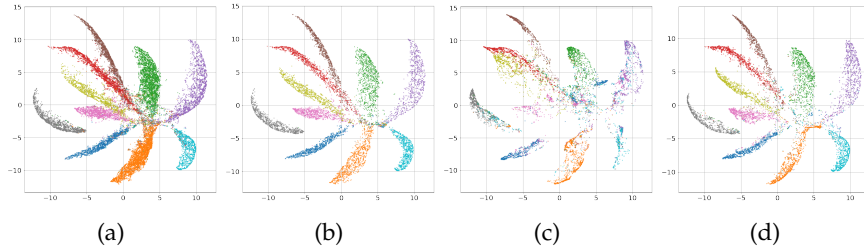


Fig. 2: UMAP visualization for the $\mathcal{S} \rightarrow \mathcal{M}$ task: (a) the source domain testing split, (b) the internal distribution samples, (c) the target domain testing split prior to adaptation, and (d) post adaptation. (Best viewed in color).

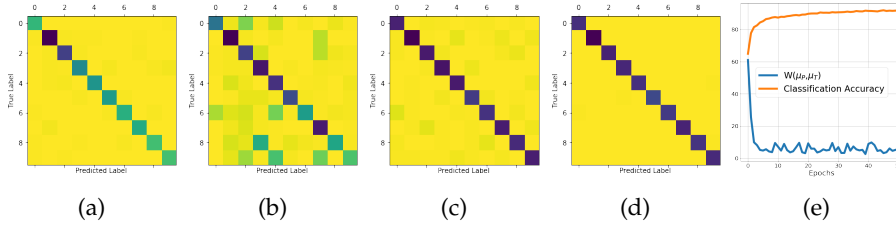


Fig. 3: Confusion matrices for the $\mathcal{S} \rightarrow \mathcal{M}$ task: (a) the source domain (b) the target domain prior to adaptation, (c) the target domain after adaptation, (d) the target domain with a model trained using the target fully labeled dataset, and (e) the cross-domain distribution & the test error vs learning iterations. (Best viewed enlarged on screen and in color).

(Figures 3d). This observation is predictable from Theorem 1 because the model performance on the target domain is upperbounded by the source domain error.

We have also validated Theorem 1 in terms of effect of SMAUI on performance in the target domain in Figure 3e. We have plotted the test error versus optimization epochs during training. We observe that as more training epochs are performed and the distributions are aligned, i.e., domain discrepancy is minimized, the testing accuracy on the target domain accuracy constantly increases. This accords with Eq. (4) because SMAUI gradually aligns the target domain distribution with the source distribution using the internal distribution.

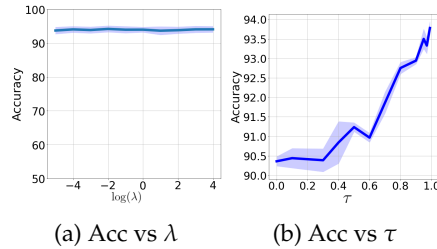


Fig. 4: Hyperparameter analysis study.

A point of strength for our algorithm is that there are only two major algorithm-specific hyper-parameters: λ and τ . As a result, extensive hyper-parameter tuning is not required. We have studied the effect of the value for these hyper-parameters on the classification performance for the task $\mathcal{S} \rightarrow \mathcal{M}$ in Figure 4. In this figure, the dark curve denotes the average performance over 5 runs and the lighter shaded region denotes the standard deviation. We observed that the algorithm performance is stable with respect to the value of trade-off parameter λ . This is not surprising because in Eq. (3), the $\mathcal{L}(\cdot)$ loss term is small due to initial training on the source domain from the beginning and the dominant term is the domain-alignment term. We also observe in Figure 4b that the performance improves when the value of the confidence parameter is $\tau \approx 1$. This observation accords with our deduction in Theorem 1, predictable from Eq. (4). We conclude that the empirical results support our theorem.

7 Conclusions

We addressed the problem of model adaptation in a sequential task learning setting. Our algorithm is based on minimizing the distributional domain discrepancy in a shared embedding space using an intermediate multi-modal internal distribution. We estimate this distribution using a GMM distribution. The internal distribution encodes what has been learned from the source domain. As a result, we can adapt the source-trained classifier using this distribution to generalize better on the target domain. A future research direction is to improve the algorithm is equipping it with class-conditional alignment techniques.

References

1. Xavier Glorot, Antoine Bordes, and Yoshua Bengio. Domain adaptation for large-scale sentiment classification: a deep learning approach. In *Proceedings of the 28th International Conference on Machine Learning*, pages 513–520, 2011.
2. Hal Daumé III. Frustratingly easy domain adaptation. In *Proceedings of the 45th Annual Meeting of the Association of Computational Linguistics*, pages 256–263, 2007.
3. Kaiming He, Xiangyu Zhang, Shaoqing Ren, and Jian Sun. Deep residual learning for image recognition. In *Proceedings of the IEEE Conference on Computer Vision and Pattern Recognition*, pages 770–778, 2016.
4. Swami Sankaranarayanan, Yogesh Balaji, Carlos D Castillo, and Rama Chellappa. Generate to adapt: Aligning domains using generative adversarial networks. In *Proceedings of CVPR*, pages 8503–8512, 2018.
5. Zhongyi Pei, Zhangjie Cao, Mingsheng Long, and Jianmin Wang. Multi-adversarial domain adaptation. In *Proceedings Thirty-Second AAAI Conference on Artificial Intelligence*, pages 3934–3941, 2018.
6. Yabin Zhang, Hui Tang, Kui Jia, and Mingkui Tan. Domain-symmetric networks for adversarial domain adaptation. In *Proceedings of the IEEE Conference on Computer Vision and Pattern Recognition*, pages 5031–5040, 2019.
7. Mingsheng Long, Zhangjie Cao, Jianmin Wang, and Michael I Jordan. Conditional adversarial domain adaptation. In *Advances in Neural Information Processing Systems*, pages 1640–1650, 2018.

8. Mingsheng Long, Yue Cao, Jianmin Wang, and Michael Jordan. Learning transferable features with deep adaptation networks. In *Proceedings of International Conference on Machine Learning*, pages 97–105, 2015.
9. Yaroslav Ganin and Victor Lempitsky. Unsupervised domain adaptation by back-propagation. In *Proceedings of ICML*, pages 1180–1189, 2015.
10. Mingsheng Long, Han Zhu, Jianmin Wang, and Michael I Jordan. Deep transfer learning with joint adaptation networks. In *Proceedings of the 34th International Conference on Machine Learning-Volume 70*, pages 2208–2217. JMLR. org, 2017.
11. Guoliang Kang, Lu Jiang, Yi Yang, and Alexander G Hauptmann. Contrastive adaptation network for unsupervised domain adaptation. In *Proceedings of the IEEE Conference on Computer Vision and Pattern Recognition*, pages 4893–4902, 2019.
12. Mohammad Rostami, Soheil Kolouri, Eric Eaton, and Kyungnam Kim. Deep transfer learning for few-shot sar image classification. *Remote Sensing*, 11(11):1374, 2019.
13. Mohammad Rostami, Soheil Kolouri, Praveen K Pilly, and James McClelland. Generative continual concept learning. In *AAAI*, pages 5545–5552, 2020.
14. Ian Goodfellow, Jean Pouget-Abadie, Mehdi Mirza, Bing Xu, David Warde-Farley, Sherjil Ozair, Aaron Courville, and Yoshua Bengio. Generative adversarial nets. In *Advances in Neural Information Processing Systems*, pages 2672–2680, 2014.
15. Kevin Roth, Aurelien Lucchi, Sebastian Nowozin, and Thomas Hofmann. Stabilizing training of generative adversarial networks through regularization. In *Advances in Neural Information Processing Systems*, pages 2018–2028, 2017.
16. Luke Metz, Ben Poole, David Pfau, and Jascha Sohl-Dickstein. Unrolled generative adversarial networks. In *ICLR*, pages 1–14, 2017.
17. Jogendra Nath Kundu, Naveen Venkat, R Venkatesh Babu, et al. Universal source-free domain adaptation. In *Proceedings of the IEEE/CVF Conference on Computer Vision and Pattern Recognition*, pages 4544–4553, 2020.
18. Rui Li, Qianfen Jiao, Wenming Cao, Hau-San Wong, and Si Wu. Model adaptation: Unsupervised domain adaptation without source data. In *Proceedings of the IEEE/CVF Conference on Computer Vision and Pattern Recognition*, pages 9641–9650, 2020.
19. Baochen Sun and Kate Saenko. Deep coral: Correlation alignment for deep domain adaptation. In *European conference on computer vision*, pages 443–450. Springer, 2016.
20. Nicolas Courty, Rémi Flamary, Devis Tuia, and Alain Rakotomamonjy. Optimal transport for domain adaptation. *IEEE Transactions on Pattern Analysis and Machine Intelligence*, 39(9):1853–1865, 2016.
21. Bharath Bhushan Damodaran, Benjamin Kellenberger, Rémi Flamary, Devis Tuia, and Nicolas Courty. Deepjdot: Deep joint distribution optimal transport for unsupervised domain adaptation. In *Proceedings of the European Conference on Computer Vision (ECCV)*, pages 447–463, 2018.
22. Chen-Yu Lee, Tanmay Batra, Mohammad Haris Baig, and Daniel Ulbricht. Sliced wasserstein discrepancy for unsupervised domain adaptation. In *Proceedings of the IEEE Conference on Computer Vision and Pattern Recognition*, pages 10285–10295, 2019.
23. Mark Dredze and Koby Crammer. Online methods for multi-domain learning and adaptation. In *Proceedings of the Conference on Empirical Methods in Natural Language Processing*, pages 689–697. Association for Computational Linguistics, 2008.
24. V Jain and E Learned-Miller. Online domain adaptation of a pre-trained cascade of classifiers. In *Proceedings of CVPR*, pages 577–584, 2011.
25. Dongrui Wu. Online and offline domain adaptation for reducing bci calibration effort. *IEEE Transactions on Human-Machine Systems*, 47(4):550–563, 2016.
26. N. Bonnotte. *Unidimensional and evolution methods for optimal transportation*. PhD thesis, Paris 11, 2013.

27. Y. Ganin, E. Ustinova, H. Ajakan, P. Germain, H. Larochelle, F. Laviolette, M. Marchand, and V. Lempitsky. Domain-adversarial training of neural networks. *The Journal of Machine Learning Research*, 17(1):2096–2030, 2016.
28. Eric Tzeng, Judy Hoffman, Kate Saenko, and Trevor Darrell. Adversarial discriminative domain adaptation. In *Proceedings of the IEEE Conference on Computer Vision and Pattern Recognition*, pages 7167–7176, 2017.
29. Xinhong Ma, Tianzhu Zhang, and Changsheng Xu. Deep multi-modality adversarial networks for unsupervised domain adaptation. *IEEE Transactions on Multimedia*, 21(9):2419–2431, 2019.
30. Muhammad Ghifary, W Bastiaan Kleijn, Mengjie Zhang, David Balduzzi, and Wen Li. Deep reconstruction-classification networks for unsupervised domain adaptation. In *European Conference on Computer Vision*, pages 597–613. Springer, 2016.
31. Baochen Sun, Jiashi Feng, and Kate Saenko. Return of frustratingly easy domain adaptation. In *Proceedings of the AAAI Conf. on Artificial Intelligence*, volume 30, 2016.
32. Jian Shen, Yanru Qu, Weinan Zhang, and Yong Yu. Wasserstein distance guided representation learning for domain adaptation. In *Proceedings of the AAAI Conference on Artificial Intelligence*, volume 32, 2018.
33. Chao Chen, Zhihong Chen, Boyuan Jiang, and Xinyu Jin. Joint domain alignment and discriminative feature learning for unsupervised deep domain adaptation. In *Proc. of the AAAI Conf. on Artificial Intelligence*, volume 33, pages 3296–3303, 2019.
34. Mengxue Li, Yi-Ming Zhai, You-Wei Luo, Peng-Fei Ge, and Chuan-Xian Ren. Enhanced transport distance for unsupervised domain adaptation. In *Proceedings of the IEEE/CVF Conf. on Computer Vision and Pattern Recognition*, pages 13936–13944, 2020.
35. Jian Liang, Dapeng Hu, and Jiashi Feng. Do we really need to access the source data? source hypothesis transfer for unsupervised domain adaptation. In *International Conference on Machine Learning*, pages 6028–6039. PMLR, 2020.
36. Konstantinos Bousmalis, George Trigeorgis, Nathan Silberman, Dilip Krishnan, and Dumitru Erhan. Domain separation networks. In *Advances in Neural Information Processing Systems*, pages 343–351, 2016.
37. Judy Hoffman, Eric Tzeng, Taesung Park, Jun-Yan Zhu, Phillip Isola, Kate Saenko, Alexei Efros, and Trevor Darrell. CyCADA: Cycle-consistent adversarial domain adaptation. In *International Conference on Machine Learning*, pages 1989–1998, 2018.
38. Vivien Seguy, Bharath Bhushan Damodaran, Remi Flamary, Nicolas Courty, Antoine Rolet, and Mathieu Blondel. Large-scale optimal transport and mapping estimation. In *ICLR*, 2018.
39. Pedro O Pinheiro. Unsupervised domain adaptation with similarity learning. In *Proceedings of the IEEE Conference on Computer Vision and Pattern Recognition*, pages 8004–8013, 2018.
40. Kuniaki Saito, Kohei Watanabe, Yoshitaka Ushiku, and Tatsuya Harada. Maximum classifier discrepancy for unsupervised domain adaptation. In *Proceedings of the IEEE Conference on Computer Vision and Pattern Recognition*, pages 3723–3732, 2018.
41. Leland McInnes, John Healy, Nathaniel Saul, and Lukas Großberger. UMAP: Uniform manifold approximation and projection. *Journal of Open Source Soft.*, 3(29):861, 2018.
42. R. Neal. Slice sampling. *Annals of statistics*, pages 705–741, 2003.
43. S. Helgason. The radon transform on \mathbb{R}^n . In *Integral Geometry and Radon Transforms*, pages 1–62. Springer, 2011.
44. A. Redko, I. and Habrard and M. Sebban. Theoretical analysis of domain adaptation with optimal transport. In *Joint European Conference on Machine Learning and Knowledge Discovery in Databases*, pages 737–753. Springer, 2017.

45. François Bolley, Arnaud Guillin, and Cédric Villani. Quantitative concentration inequalities for empirical measures on non-compact spaces. *Probability Theory and Related Fields*, 137(3-4):541–593, 2007.

A Appendix: Sliced Wasserstein distance

In our work, we have used the Sliced Wasserstein (SWD) distance for measuring distribution discrepancy. We provide a short background for the interested reader here. SWD is defined based on the Wasserstein distance (WD). The Wasserstein distance between two probability distributions p_S and p_T , can be defined as:

$$W_c(p_S, p_T) = \inf_{\gamma \in \Gamma(p_S, p_T)} \int_{X \times Y} c(x, y) d\gamma(x, y) \quad (5)$$

where $\Gamma(p_S, p_T)$ is the set of all joint distributions $p_{S,T}$ with marginal single variable distributions p_S and p_T , and $c : X \times Y \rightarrow \mathbb{R}^+$ is the transportation cost which normally is assumed to be ℓ_2 -norm Euclidean distance. As can be seen, computing the Wasserstein distance is not trivial and requires solving an optimization problem which is a special case of linear programming problems as the subjective function in Eq. (5) and the constraint on γ are both linear. However, when the distributions are 1-dimensional, computing the Wasserstein distance reduces to a closed-form solution as follows:

$$W_c(p_S, p_T) = \int_0^1 c(P_S^{-1}(\tau), P_T^{-1}(\tau)) d\tau, \quad (6)$$

where P_S and P_T are the cumulative distributions of the 1-dimensional distributions p_S and p_T . This closed-form solution that has a much lower computational complexity compared to Eq. (5), motivates the definition of SWD in order to extend application of Eq.(6) on higher dimensional distributions.

The idea behind the SWD is based on the slice sampling [42]. The idea is to project two d -dimensional probability distributions into their marginal one-dimensional distributions, i.e., slicing the high-dimensional distributions, and to approximate the Wasserstein distance by integrating the Wasserstein distances between the resulting 1-dimensional marginal probability distributions over all possible one-dimensional subspaces, which have closed form solution. This can be a good estimate for the optimal transport as any probability distribution can be represented uniquely via the set of 1-dimensional marginal projection distributions [43]. For the distribution p_S , a one-dimensional slice of the distribution is defined:

$$\mathcal{R}p_S(t; \gamma) = \int_{S^{d-1}} p_S(\mathbf{x}) \delta(t - \langle \gamma, \mathbf{x} \rangle) d\mathbf{x}, \quad (7)$$

where $\delta(\cdot)$ denotes the Kronecker delta function, $\langle \cdot, \cdot \rangle$ denotes the vector inner dot product, S^{d-1} is the d -dimensional unit sphere, and γ is the projection direction. In other words, $\mathcal{R}p_S(\cdot; \gamma)$ is a marginal distribution of p_S obtained from integrating p_S over the hyperplanes orthogonal to γ . The SWD then is defined as integral of the Wasserstein distance between the sliced distributions over all 1-dimensional subspaces γ on the unit sphere:

$$SW(p_S, p_T) = \int_{S^{d-1}} W(\mathcal{R}p_S(\cdot; \gamma), \mathcal{R}p_T(\cdot; \gamma)) d\gamma \quad (8)$$

where $W(\cdot)$ denotes the Wasserstein distance. The main advantage of using the SWD is that as evident from Eq (8), unlike the Wasserstein distance, calculation of the SWD does not require a numerically expensive optimization. This is due to the fact that the Wasserstein distance between two one-dimensional probability distributions has a closed form solution. Since only samples from distributions are available, the one-dimensional Wasserstein distance can be approximated as the ℓ_p -distance between the sorted samples. Note however, this way we can compute merely the integrand function in Eq. (8) for a known γ . To approximate the integral in Eq. (8), we can use a Monte Carlo style integration. First, we sample the projection subspace γ from a uniform distribution that is defined over the unit sphere and then compute 1-dimensional Wasserstein distance on the sample. We can then approximate the integral in Eq. (8) by computing the arithmetic average over a suitably large enough number of drawn samples. Formally, the SWD between f -dimensional samples $\{\phi(\mathbf{x}_i^S) \in \mathbb{R}^f \sim p_S\}_{i=1}^M$ and $\{\phi(\mathbf{x}_i^T) \in \mathbb{R}^f \sim p_T\}_{i=1}^M$ in our problem of interest can be approximated as the following sum:

$$SW^2(p_S, p_T) \approx \frac{1}{L} \sum_{l=1}^L \sum_{i=1}^M |\langle \gamma_l, \phi(\mathbf{x}_{s_l[i]}^S) \rangle - \langle \gamma_l, \phi(\mathbf{x}_{t_l[i]}^T) \rangle|^2 \quad (9)$$

where $\gamma_l \in \mathcal{S}^{f-1}$ is uniformly drawn random sample from the unit f -dimensional ball \mathcal{S}^{f-1} , and $s_l[i]$ and $t_l[i]$ are the sorted indices of $\{\gamma_l \cdot \phi(\mathbf{x}_i)\}_{i=1}^M$ for source and target domains, respectively. We utilize the empirical version of SWD in Eq. (9) as the discrepancy measure between the probability distributions to match them in the embedding space. Note that the function in Eq. (9) is differentiable with respect to the encoder parameters and hence we can use gradient-based optimization techniques that are commonly used in deep learning to minimize it with respect to the model parameters.

B Appendix: Proof of Theorem 1

We first note that When we generate the pseudo-dataset, we ensure to select pseudo-data points for which the model is confident. To this end, we pick a threshold τ , draw random pseudo-data points z_i^p , and pass them through the classifier sub-network. We then look at the predicted label distribution at the final softmax layer and include only those data-points for which the model is confident with prediction probability greater than τ . Let $e_{\mathcal{P}}$ denotes the true risk of the initial optimal model that is trained using the source domain data on the generated pseudo-dataset.

We benefit from the following theorem by Redko et al. [44] in our proof.

Theorem 2 (Redko et al. [44]): Under the assumptions described in our framework, assume that a model is trained on the source domain, then for any $d' > d$ and $\zeta < \sqrt{2}$, there exists a constant number N_0 depending on d' such that for any $\epsilon > 0$ and $\min(N, M) \geq \max(\epsilon^{-d'}, \epsilon^{-d'+2})$ with probability at least

$1 - xi$, the following holds:

$$e_{\mathcal{T}} \leq e_{\mathcal{S}} + W(\hat{\mu}_{\mathcal{T}}, \hat{\mu}_{\mathcal{S}}) + e_{\mathcal{C}}(\mathbf{w}^*) + \sqrt{(2 \log(\frac{1}{xi})/\zeta)} \left(\sqrt{\frac{1}{N}} + \sqrt{\frac{1}{M}} \right). \quad (10)$$

Theorem 2 provides an upperbound for the performance of the source domain trained model on the target domain. We use Theorem 2 to deduce Theorem 1. Redko et al. [44] prove Theorem 2 for a binary classification setting in a joint training UDA setting. We also provide our proof in this case but it can be conveniently extended.

Theorem 1 : Consider that we generate a pseudo-dataset using the internal distribution and update the model for sequential UDA using SMAUP algorithm. Then, the following holds:

$$e_{\mathcal{T}} \leq e_{\mathcal{S}} + W(\hat{\mu}_{\mathcal{S}}, \hat{\mu}_{\mathcal{P}}) + W(\hat{\mu}_{\mathcal{T}}, \hat{\mu}_{\mathcal{P}}) + (1 - \tau) + e_{\mathcal{C}'}(\mathbf{w}^*) + \sqrt{(2 \log(\frac{1}{xi})/\zeta)} \left(\sqrt{\frac{1}{N}} + \sqrt{\frac{1}{M}} + 2\sqrt{\frac{1}{N_p}} \right), \quad (11)$$

where xi is a constant which depends on $\mathcal{L}(\cdot)$ and $e_{\mathcal{C}'}(\mathbf{w}^*)$ denotes the expected risk of the optimally joint trained model when used on both the source domain and the pseudo-dataset.

Proof: Since the parameter τ denotes the threshold that we use to select the pseudo-data points in the embedding space, then the probability that the predicted labels for the pseudo-data points to be false by this model is equal to $1 - \tau$. We can define the following difference for the pseudo-data points:

$$|\mathcal{L}(h_{\mathbf{w}_0}(z_i^p), \mathbf{y}_i^p) - \mathcal{L}(h_{\mathbf{w}_0}(z_i^p), \hat{\mathbf{y}}_i^p)| = \begin{cases} 0, & \text{if } \mathbf{y}_i^t = \hat{\mathbf{y}}_i^t. \\ 1, & \text{otherwise.} \end{cases} \quad (12)$$

Hence, using Jensen's inequality and by applying the expectation operator on the above error can be computed as:

$$|e_{\mathcal{P}} - e_{\mathcal{T}}| \leq \mathbb{E}(|\mathcal{L}(h_{\mathbf{w}_0}(z_i^p), \mathbf{y}_i^p) - \mathcal{L}(h_{\mathbf{w}_0}(z_i^p), \hat{\mathbf{y}}_i^p)|) \leq (1 - \tau). \quad (13)$$

Using Eq. (13) we can deduce:

$$e_{\mathcal{S}} + e_{\mathcal{T}} = e_{\mathcal{S}} + e_{\mathcal{T}} + e_{\mathcal{P}} - e_{\mathcal{P}} \leq e_{\mathcal{S}} + e_{\mathcal{P}} + |e_{\mathcal{T}} - e_{\mathcal{P}}| \leq e_{\mathcal{S}} + e_{\mathcal{P}} + (1 - \tau). \quad (14)$$

Note that since Eq. (14) is valid for all \mathbf{w} , if we consider the joint optimal parameter \mathbf{w}^* in the right-hand and the left-hand sides of Eq. (14), we deduce:

$$e_{\mathcal{C}}(\mathbf{w}^*) \leq e_{\mathcal{C}'}(\mathbf{w}) + (1 - \tau). \quad (15)$$

Now by considering Theorem 2 for the the source and the target domains and then applying Eq. (15) on Eq.(10), we have:

$$e_{\mathcal{T}} \leq e_{\mathcal{S}} + W(\hat{\mu}_{\mathcal{T}}, \hat{\mu}_{\mathcal{S}}) + e'_C(\mathbf{w}^*) + (1 - \tau) + \sqrt{(2 \log(\frac{1}{\xi_i})/\zeta)} (\sqrt{\frac{1}{N}} + \sqrt{\frac{1}{M}}). \quad (16)$$

We used Eq. (16) to deduce Theorem 1 by relating the terms to the internal distribution.

We first use the triangular inequality on the WD metric to deduce the following relation for the $W(\hat{\mu}_{\mathcal{T}}, \hat{\mu}_{\mathcal{S}})$ term in Eq. (16):

$$W(\hat{\mu}_{\mathcal{T}}, \hat{\mu}_{\mathcal{S}}) \leq W(\hat{\mu}_{\mathcal{T}}, \mu_{\mathcal{P}}) + W(\hat{\mu}_{\mathcal{S}}, \mu_{\mathcal{P}}) \leq W(\hat{\mu}_{\mathcal{T}}, \hat{\mu}_{\mathcal{P}}) + W(\hat{\mu}_{\mathcal{S}}, \hat{\mu}_{\mathcal{P}}) + 2W(\hat{\mu}_{\mathcal{P}}, \mu_{\mathcal{P}}). \quad (17)$$

We can simplify the term $W(\hat{\mu}_{\mathcal{P}}, \mu_{\mathcal{P}})$ in the above using Theorem 1.1 in the work by Bolley et al. [45].

Theorem 3 (Theorem 1.1 by Bolley et al. [45]): consider that $p(\cdot) \in \mathcal{P}(\mathcal{Z})$ and $\int_{\mathcal{Z}} \exp(\alpha \|\mathbf{x}\|_2^2) dp(\mathbf{x}) < \infty$ for some $\alpha > 0$. Let $\hat{p}(\mathbf{x}) = \frac{1}{N} \sum_i \delta(\mathbf{x}_i)$ denote the empirical distribution that is built from the samples $\{\mathbf{x}_i\}_{i=1}^N$ that are drawn i.i.d from $\mathbf{x}_i \sim p(\mathbf{x})$. Then for any $d' > d$ and $\xi_i < \sqrt{2}$, there exists N_0 such that for any $\epsilon > 0$ and $N \geq N_0 \max(1, \epsilon^{-(d'+2)})$, we have:

$$P(W(p, \hat{p}) > \epsilon) \leq \exp(-\frac{\xi_i}{2} N \epsilon^2) \quad (18)$$

This relation measure the distance between the estimated empirical distribution and the true distribution in terms of the WD distance. We can use it estimate the error between the true and the empirical distribution in terms of the distribution samples used for empirical estimation to simplify $W(\hat{\mu}_{\mathcal{P}}, \mu_{\mathcal{P}})$ in Eq. (16).

Finally, replacing Eq. (17) and Eq. (18) in the corresponding terms Eq. (16), concludes Theorem 2 as stated:

$$e_{\mathcal{T}} \leq e_{\mathcal{S}} + W(\hat{\mu}_{\mathcal{S}}, \hat{\mu}_{\mathcal{P}}) + W(\hat{\mu}_{\mathcal{T}}, \hat{\mu}_{\mathcal{P}}) + (1 - \tau) + e'_C(\mathbf{w}^*) + \sqrt{(2 \log(\frac{1}{\xi_i})/\zeta)} (\sqrt{\frac{1}{N}} + \sqrt{\frac{1}{M}} + 2\sqrt{\frac{1}{N_p}}), \quad (19)$$

C Appendix: Details of Experimental Implementation

In the digit recognition experiments, we resized the images of SVHN dataset to 28×28 images to have the same size of the MNIST and the USPS datasets. This is necessary because we use the same encoder across all domains.

In our experiments, we used cross entropy loss as the discrimination loss. At each training epoch, we computed the combined loss function on the training split of data and stopped training when the loss function became constant.

We used Keras for implementation and ADAM optimizer with learning rate $lr = 10^{-4}$. We have run our code on a cluster node equipped with 2 Nvidia Tesla P100-SXM2 GPU's. The implemented code is provided as a supplement.

All the datasets have their own standard training/testing splits in all domains. For each experiment, we used these testing splits to measure performance of the methods that we report in terms of classification accuracy. We used the classification rate on the testing set to measure performance of the algorithms. We performed 10 training trials and reported the average performance and the standard deviation on the testing sets for these trials.